Journal of Power Sources 198 (2012) 264–272

Contents lists available at SciVerse ScienceDirect

Journal of Power Sources

journal homepage: www.elsevier.com/locate/jpowsour

Electrophoretic deposition of lithium iron phosphate cathode for thin-film 3D-microbatteries

H. Mazor[a,*], D. Golodnitsky[a,b], L. Burstein[b], A. Gladkich[c], E. Peled[a]

[a] School of Chemistry, Tel Aviv University, Tel Aviv 69978, Israel
[b] Wolfson Applied Materials Research Center, Tel Aviv University, Tel Aviv 69978, Israel
[c] Micron Semiconductor, Israel

ARTICLE INFO

Article history:
Received 26 July 2011
Received in revised form
18 September 2011
Accepted 27 September 2011
Available online 12 October 2011

Keywords:
Li-ion microbattery
Advanced cathode materials
Electrophoretic deposition
Lithium iron phosphate

ABSTRACT

An electrophoretic deposition (EPD) method has been developed for the first time to prepare thin-film $LiFePO_4$ cathodes. The effects of polymers and surface-active additives in the electrolytic bath, voltage and deposition protocol have been studied with the aim of obtaining highly adhesive, compact pristine $LiFePO_4$ and polymer–$LiFePO_4$ composite films to be utilized in planar and three-dimensional microbatteries. The samples were investigated by scanning electron microscopy (SEM), energy-dispersive X-ray spectroscopy (EDX), XPS and TOFSIMS. These methods confirmed the presence of a polymer binder and its homogeneous lateral distribution in the composite EPD-$LiFePO_4$ cathode. Li/$LiFePO_4$ semi-3D concentric microbatteries (3DCMB) on perforated silicon substrates showed a peak-pulse-power capability of 175 mW cm^{-2} and stable electrochemical behavior for over 200 cycles at 100% DOD. Coating the $LiFePO_4$ with a thin layer of copper sulfide improved the cell performance even more. The 3D-$LiFePO_4$–CuS-coated batteries are capable of delivering peak pulse power greater than 200 mW cm^{-2} and an energy density of 6–10 mWh cm^{-2} – adequate for the needs of microsystems.

1. Introduction

Recent advances in the technology of micro-systems have not been matched by similar progress in battery technology and, as a result, the battery is often larger than the system itself. Recently suggested 3D architectures of microbatteries offer a new approach for miniaturizing power sources [1–5]. These batteries are designed to have a small footprint and yet provide sufficient power and energy to operate autonomous MEMS and implantable medical devices. One approach for fabricating such batteries is to utilize the "inner" volume of the silicon or glass substrate by perforating it with high-aspect-ratio through microchannels [4–7]. The substrate consists of 8000–30,000 cylindrical through-holes per cm^2 with a complete lithium-battery unit inside each channel, all connected in parallel. The 3D-concentric microbattery (3D-CMB) is made of several conformal thin-films of nanosize materials: a current collector, a cathode, a hybrid polymer electrolyte (HPE) and a lithiated-graphite anode [5–8]. The schematic presentation of such a 3D-structure is shown in Fig. 1 [7].

Most of the thin-film electrode materials used in current commercial variations of thin-film batteries are deposited in vacuum chambers by RF and DC magnetron sputtering and by thermal evaporation on to unheated substrates. In addition, many publications report exploring a variety of physical and chemical vapor-deposition processes, such as pulsed-laser deposition, electron cyclotron resonance sputtering, and aerosol spray coating for one or more components of the battery [9]. Physical vapor-deposition methods do not provide coating of high-aspect-ratio substrates and chemical vapor-deposition is a relatively slow process and requires costly equipment.

We have recently developed an inexpensive and relatively simple electrodeposition method for the preparation of 3D molybdenum oxysulfide, iron oxysulfide, vanadium pentoxide and copper sulfide cathodes [10,11]. While 3D-CMBs with these cathodes showed stable electrochemical behavior and high capacity retention, none of these materials contain lithium and, therefore, prelithiation of the graphite-based anode is essential.

Among the available cathode materials, the iron-based orthophosphate $LiFePO_4$, with a theoretical specific capacity of 170 mAh g^{-1}, is an ideal cathode material for lithium-ion batteries because of its high power capability, excellent cycle life, safety and non-toxicity [12–15]. However, its intrinsically low electronic conductivity of about 10^{-9} S cm^{-1} is an adversity that needs to overcome [16]. The strategies to improve the properties

* Corresponding author. Tel.: +972 3 640 7820.
E-mail addresses: hadarmaz@tau.ac.il (H. Mazor), golod@tau.ac.il (D. Golodnitsky).

0378-7753/$ – see front matter © 2011 Elsevier B.V. All rights reserved.
doi:10.1016/j.jpowsour.2011.09.108

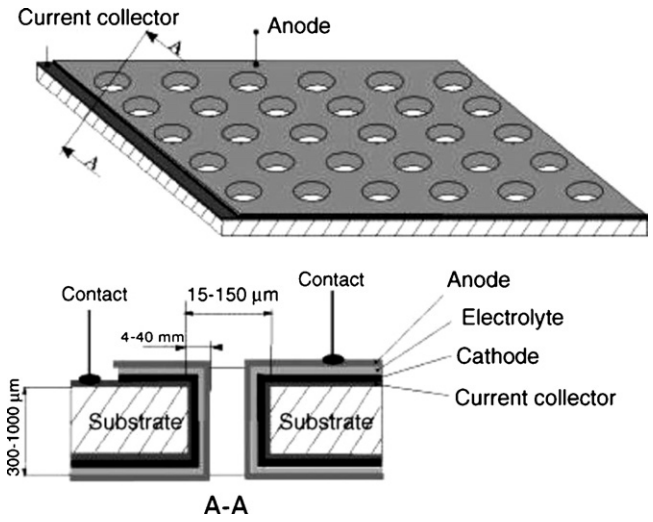

Fig. 1. Schematic presentation of the 3D microbattery.

of $LiFePO_4$ include the synthesis of nanocrystalline particles [17,18], ion doping [19,20], carbon coating [21], and metal oxide (i.e. V_2O_3) with high electronic conductivity as third-phase modification of $LiFePO_4$/C particles [22]. Preparation of a carbon-coated lithium iron phosphate (C–$LiFePO_4$)/polypyrrole (PPy) composite cathode by cyclic voltammetry has been recently reported [23,24].

This work addresses, for the first time, the feasibility of an electrophoretic deposition method for the preparation of a lithium iron phosphate cathode and the structural and electrochemical characterization of such a cathode in planar and semi-3D microbattery configurations.

2. Experimental

$LiFePO_4$ powder (was kindly donated by Hydro-Quebec, Quebec, Canada), black-pearl carbon (BP) and PVDF were dispersed in an acetone solution containing 0.28 mg L^{-1} I_2 at a ratio of $LiFePO_4$:BP:PVDF of 91:4:5, %(w/w). Then 0.4% (v/v) of the non-ionic surfactant triton X-100 (TTX ($C_{14}H_{22}O(C_2H_4O)n$)) was added to the suspension.

Pristine and modified $LiFePO_4$ (LFP) films were prepared by EPD on a planar substrate at room temperature. A nickel disk was used as the substrate (working electrode) and the counter electrode was a graphite plate. The constant voltage applied between the two electrodes was set in the range of 60–100 V for 60–120 s. Electrophoretic deposition of 3D samples was executed on gold-coated perforated-silicon substrates, which were prepared as described in [6–8]. Briefly, an inductively-coupled-plasma etching method was used to obtain 300 μm-thick perforated silicon chips with through circular channels of 50 μm diameter and 25 μm interchannel spacing (geometrical area gain (AG) = 9). This means that there are about 10,000 microbattery units connected in parallel per cm^2 of silicon footprint. An electroless method, which is able to provide conformal coatings, was used to prepare a 2 μm-thick gold current-collector high-aspect-ratio film, which coats all available surface of the substrate [25]. The gold-coated substrate was used as a working electrode sandwiched between two squares of platinum gauze, which served as counter electrodes.

Our electrophoretic deposition technique is similar to that developed by Kanamura et al. [26]. In order to improve the structural and electrochemical properties of the electrophoretically deposited cathodes, the suspension was modified by the addition of a polymer, a surface-active agent and Black-Pearl carbon for electronic conductivity enhancement. A Keithley SourceMeter model 2400 interfaced with LabTracer software and a PC was used to control the EPD process and to monitor the current and voltage profiles. The deposited samples of thin-film LFP cathodes were dried under vacuum at 120 °C for 24 h. All subsequent handling of these materials took place under an argon atmosphere in a VAC glove box containing less than 10 ppm water. For the initial 3D-cathode-feasibility tests, semi-3D-MBs were fabricated in coin cells. The semi-3D cells used in this work comprised a gold cathode-current collector, a $LiFePO_4$ cathode, a Celgard separator soaked in commercial electrolyte ($LiPF_6$ in 1:1 EC:DEC) and a lithium anode.

Planar and semi-3D electrochemical coin cells (type 2032) comprising 0.49–0.57 cm^2 lithium-metal anode, 1 M $LiPF_6$ in 1:1 EC:DEC, Celgard separator and a deposited LFP cathode, were constructed and cycled at room temperature in a Maccor series 2000 battery-test system. The polarization tests of the Li/LFP batteries were also conducted at room temperature. These measurements were carried out by applying an ascending-step current for 1 s over the range of 100 μA cm^{-2}–80 mA cm^{-2}. The batteries were allowed to rest for 20 s between steps.

A JSM-6300 scanning microscope (Jeol Co.) equipped with a Link elemental analyzer and a silicon detector, was used for the study of the surface morphology of the cathodes. X-ray-photoelectron-spectroscopy (XPS) measurements were performed under ultra-high vacuum (2.5×10^{-10} Torr base pressure) with the use of a 5600 Multi-Technique System (Physical Electronics Inc., USA). TOF SIMS tests were performed with the use of a TRIFT II (Physical Electronics Inc., USA) under the following operating conditions: primary ions In^+, DC sputtering rate 0.035 nm min^{-1} based on SiO_2 reference.

3. Results and discussion

Electrophoretic deposition is essentially a two-step process. In the first step, particles suspended in a liquid are forced to move towards an electrode by the application of an electric field to the suspension (electrophoresis). In the second step, the particles collect at one of the electrodes and form a coherent deposit on it [27]. Throwing power is defined as the ability to cover recessed portions of complexly shaped parts, is high in EPD process. This property, combined with the improved uniformity of the thickness, is a decided asset for application in 3D-MBs on high-aspect-ratio perforated substrates.

3D-lithiated cathodes, such as olivine lithium metal phosphates, $LiMPO_4$ (where metal M is iron, cobalt, manganese, nickel, vanadium, copper, titanium or a mixture of them) as well as lithium manganese oxide, lithium cobalt oxide (doped by Al, Ni, etc.) can be prepared by EPD.

Pristine and modified $LiFePO_4$ films were prepared by EPD on planar and perforated silicon substrates at room temperature. The deposition rate of the films was controlled by the concentration of the I_2 in the suspension, deposition current or potential, the amounts of active material added and binders. There is a complex interplay of all these parameters. In accordance with [26], iodine produces charged particles in the solution through a chemical reaction of I_2 with acetone. The reaction may be written as follows:

$$CH_3COCH_3 \leftrightarrow CH_3C(OH)CH_2 \quad (1)$$

$$CH_3C(OH)CH_2 + I_2 \leftrightarrow CH_3COCH_2I + H^+ + I^- \quad (2)$$

The suspensions of LFP in acetone were insufficiently stable and showed relatively rapid sedimentation when stirring was interrupted. The cathodic deposits obtained from such suspensions were highly agglomerated and non-uniform. Poor adhesion of the deposits to the nickel and gold-coated silicon substrates was observed. In general, smaller particles migrate more easily than larger particles with the same surface charge. We found that the higher the EPD voltage, the greater the number of aggregates

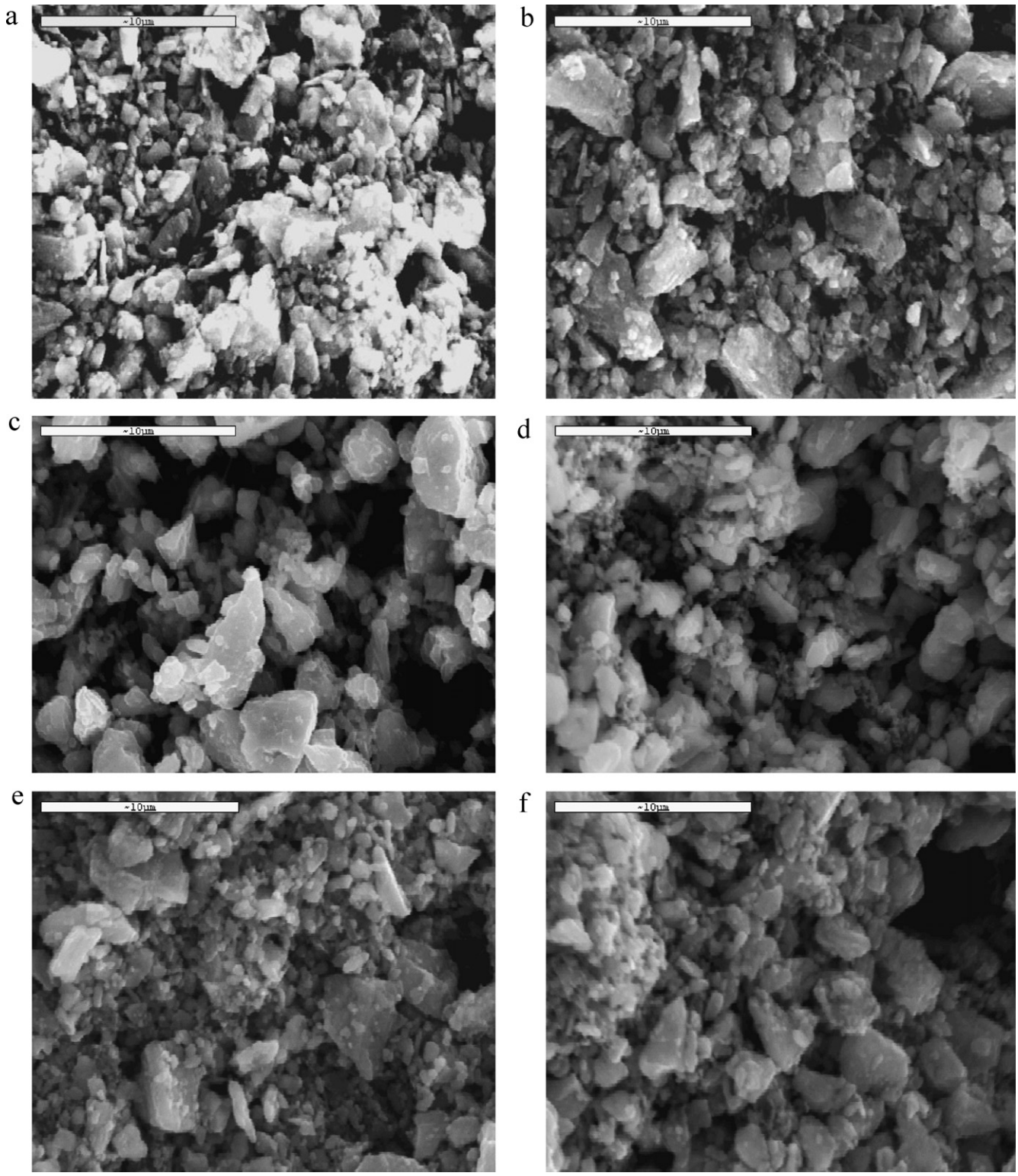

Fig. 2. SEM images of 2D cathodes at various EPD conditions; (a) pristine LFP deposited at 60 V, (b) pristine LFP deposited at 80 V, (c) LFP:BP (96:4) (w/w)% deposited at 100 V, (d) LFP:BP:PTFE (96:2:4) (w/w)% deposited at 100 V, (e) LFP:BP:PEI (87:4:9) (w/w)% deposited at 40 V and (f) LFP:BP:PEI (87:4:9) (w/w)% deposited at 100 V.

formed (Fig. 2a and b). Black-pearl carbon and polymers are used to improve the electronic conduction of LFP and the integrity of the composite cathodes in lithium-ion batteries. Addition of different polymers including Teflon (PTFE), polyethylene imine (PEI) and polyvinylidene fluoride (PVDF) to the suspension suppressed the growth of aggregates, but a few large particles still appeared in the EPD cathode film at 100 V (Fig. 2c–f). By contrast, relatively uniform deposits with smooth surface were obtained from well-dispersed and stable LFP suspensions containing Triton X-100 (TTX-100) as a dispersant (Figs. 2 and 3). TTX-100 is a nonionic surfactant which has a hydrophilic polyethylene oxide group and a hydrocarbon lipophilic group. It is used to reduce the surface tension of aqueous solutions and has the ability to solubilize molecules by causing dissociation of aggregates. The roughness of thin layers decreased in

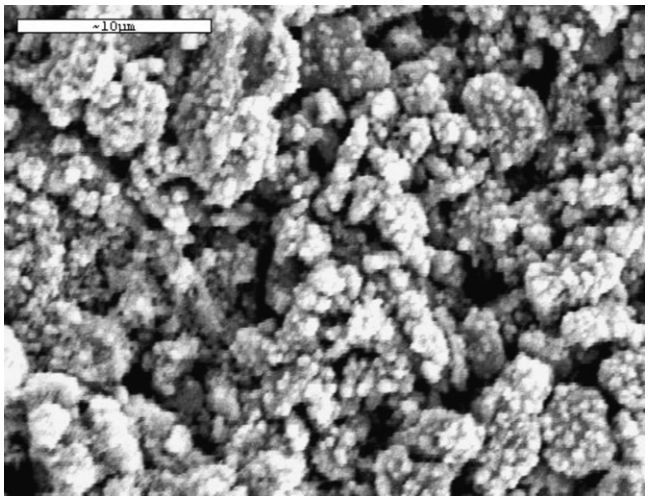

Fig. 3. SEM images of 2D modified LFP:BP:PVDF (91:4:5, (w/w)%) + TTX-100 cathodes deposited at 60 V for 60 s with topcoat of electrosynthesized thin-film CuS.

the presence of TTX-100. Modification of the electrolyte by PVDF eliminated cracks and peeling of the EPD films and enabled the preparation of 5–10 μm-thick cathode films highly adherent to the substrate. While solitary aggregates were still detected in the micrographs of modified cathodes deposited at 100 V (Fig. 4b), high-resolution SEM enabled the observation of mostly nanosize $LiFePO_4$ particles (Fig. 4d) in these cathodes. For pristine cathodes deposited even at low voltage (60 V), the generation of about 2 micron-size domains is typical (Fig. 4c).

The mass of the deposited materials increased with increase in deposition time, indicating the formation of films of different thicknesses. The mass of the pristine film was 7 mg after 60 s of EP deposition carried out at 100 V. The mass of the composite film was 6 mg after EP deposition under the same conditions, indicating a decrease in the deposition rate from the suspension containing polymer additive.

It has been shown that the electronic conductivity of the composite electrode plays a critical role in battery performance [15,28,29]. The main disadvantage of $LiFePO_4$ cathode material is its low electronic conductivity [15,28,29]. Optimization of $LiFePO_4$ for good electrochemical performance in lithium-ion batteries has been achieved by synthesizing nano-size particles and by forming a coating of electronic conductive particles, such as carbon-coating [28,29], which enhances the electronic conductivity to $0.1–10^{-4}\,S\,cm^{-1}$. The formation of nano-size $LiFePO_4$ particles makes it possible to overcome the slow ionic diffusion of Li^+. The addition of a conductive agent creates a pathway for electrons between the insulating $LiFePO_4$ particles and also between these particles and the current collector. Ideally, the electron-conducting domains should be available at every point on the

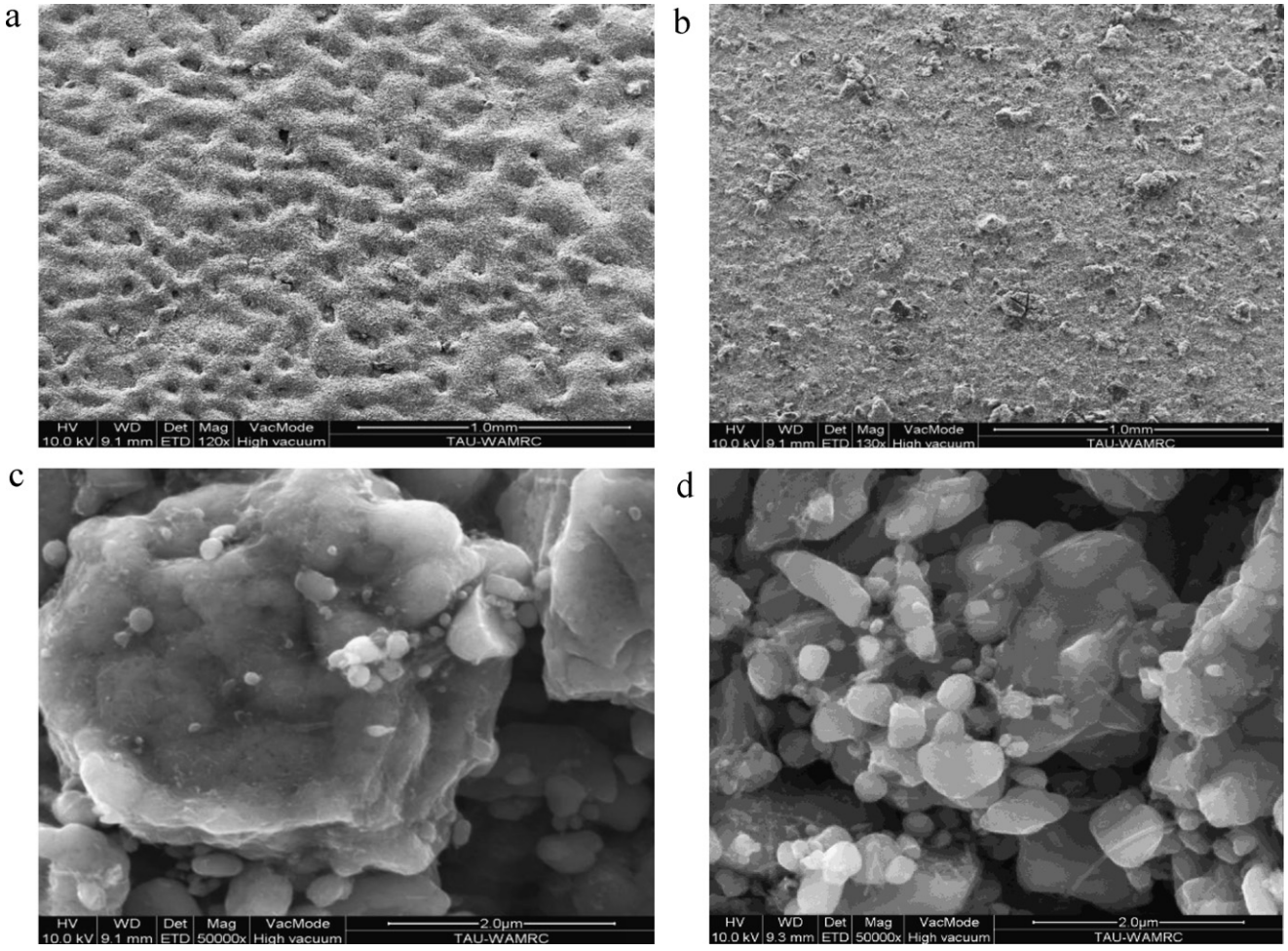

Fig. 4. HRSEM images of 2D LFP cathodes; (a) pristine LFP deposited at 60 V for 120 s at low magnification, (b) modified LFP:BP:PVDF (91:4:5, (w/w)%) + TTX-100 deposited at 100 V for 60 s at low magnification, (c) pristine LFP deposited at 60 V for 120 s at high magnification and (d) high magnification of modified LFP:BP:PVDF + TTX deposited at 100 V for 60 s.

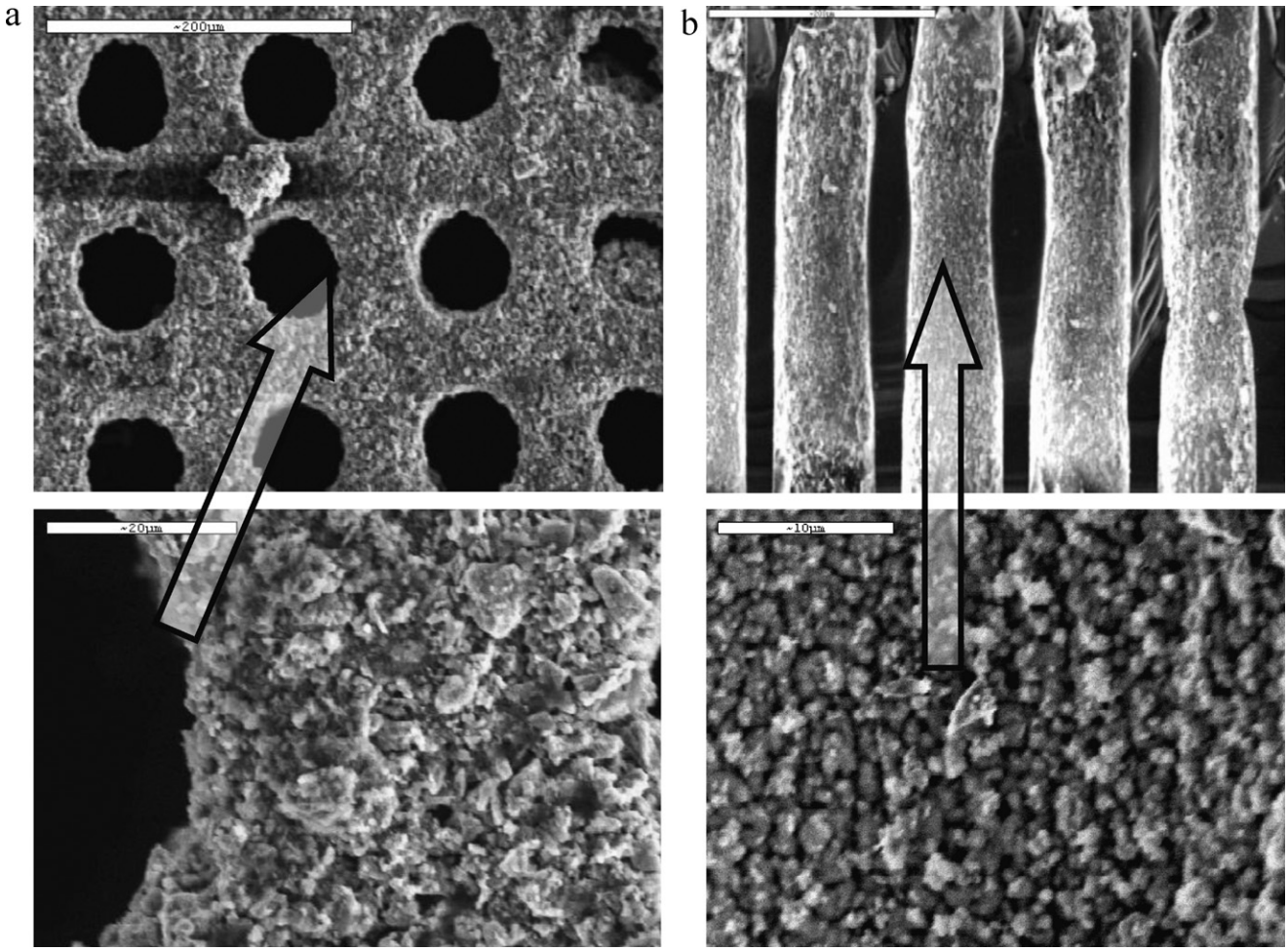

Fig. 5. SEM micrographs of modified 3D LFP-coated electrodes prepared by EPD process at 120 V for 60 s: (a) planar image of LFP-coated 3D sample (b) cross-section of channels.

surface of the particle of active electrode material (but not to block it) in order to allow the simultaneous insertion/deinsertion on the whole surface and in the bulk. In practice, however, the distribution of solids is non-uniform on both small and large scales [28,30].

Initial inhomogeneity may be caused by agglomeration of particles and by differential settling of active material, binder and conducting filler during electrode casting. These influences could contribute to non-uniform connectivity and inhomogeneous current distribution, and can even lead to electronic disconnection of portions of the electrode.

In this work we investigated an approach of improving the conductivity of composite LFP electrodes prepared by EPD. The feasibility of using, for the topcoat, material with high mixed electron/ion conductivity was tested. A thin layer of copper sulfide was electrochemically synthesized on the LFP-EPD cathode with the use of the procedure recently developed by us [10].

The morphology of the LFP cathode coated by a CuS layer about 250 nm thick (Fig. 3), resembles that of electrodeposited copper sulfide [10]. The thickness of the CuS coating, which depends on the deposition rate and time, is estimated from the results of our recent tests, described in [10].

Cross-sectional and planar SEM micrographs of the PVDF-modified LFP film deposited on the gold-coated perforated silicon chip (Fig. 5) show that the morphology of the 3D-deposit inside long narrow channels is similar to that obtained on the planar substrates. Conformal thin LFP coating was obtained throughout the silicon channel with the use of the home-made deposition setup, which provides continuous flow of the suspension.

Pristine and PVDF-modified films were further characterized by XPS, TOFSIMS and electrochemical methods. As mentioned above, the suspension for the EPD of modified films consists of $LiFePO_4$, PVDF, black-pearl carbon and TTX-100, while for the pristine sample it is composed of carbon-coated $LiFePO_4$ alone.

High-resolution XPS spectra for pristine LFP films (Fig. 6a(i)) and modified LFP films (Fig. 6a(ii)) are shown. The C1s spectrum before sputtering for the electrophoretically deposited pristine LFP film shows the presence of graphitic-like carbon on the surface (peak at 284.5 eV) resulting from the carbon coating of the LFP particles [31,32]. The new peaks that appear for the PVDF-modified film at 287 and 291 eV correspond to C–O and C–F bonds, respectively. These results confirm the existence of PVDF additive in the modified film. Fig. 6b shows XPS spectra of the pristine sample in the carbon-binding energy region before sputtering (Fig. 6b(i)) and after 4 and 10 min of Ar^+ sputtering (Fig. 6b(ii and iii, respectively)). The intensity of the C1s peak at 284.5 eV decreases with sputtering time, indicating that the carbon mainly covers the outer surface of the LFP particles as expected. The O1s spectra and P2p spectra show strong bands at 531.7 and 133.5 eV (Fig. 6c and d, respectively) due to the phosphate bonds [30]. The O1s peak at 531.7 eV (Fig. 6c) originates from the phosphate oxygen in the $LiFePO_4$ particles, while the shoulders that are seen for the modified sample (Fig. 6c(ii))

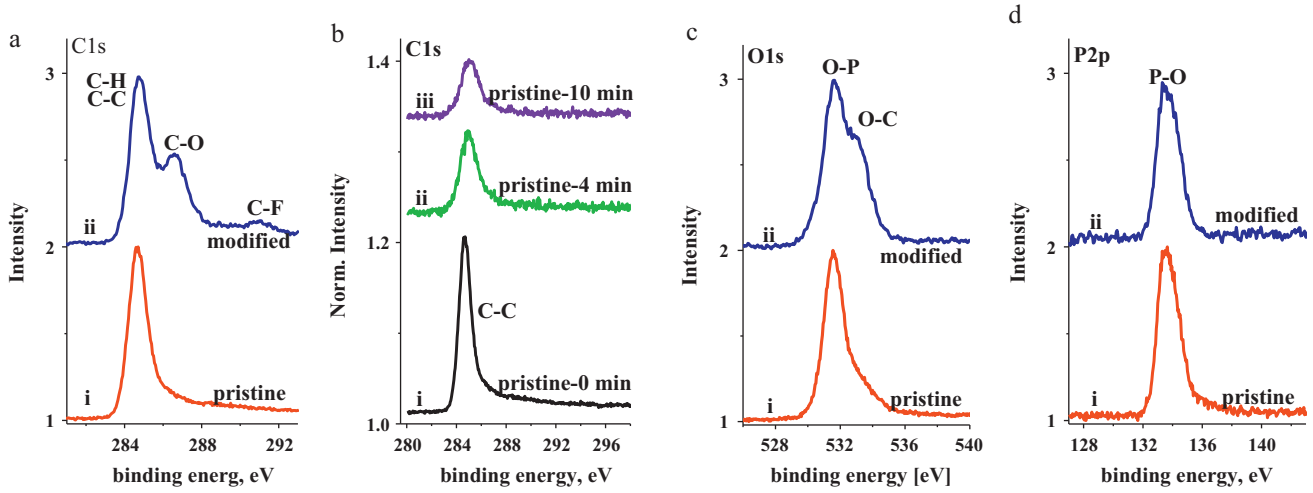

Fig. 6. XPS spectra of (a) C1s spectra for pristine and modified samples; (b) C1s spectra of pristine sample at various sputtering times; (c) O1s spectra and (d) P2p spectra for pristine and modified samples.

at 532.5–533.8 eV, may originate from polyethylene oxide group of the surfactant (TTX-100). The P2p peak (Fig. 6d) could contain overlapping contributions from $LiFePO_4$ (133.2 eV) and traces of Li_3PO_4 (133.6 eV) [28] arising *via* a surface reaction occurring during the synthesis of the particles or storage in the air.

The Fe2p spectrum (Fig. 7a) shows only the expected lines from triphyllite at 711.0 and 724.5 eV. The Li1s peak is buried under the Fe3p component (Fig. 7b) that lies in the same region at 55.5 eV [31]. Rho [30] reported that the Li1s peak was found at 56.4 eV in $LiMnPO_4$ where such an overlap does not occur. It is clear from the F1s peak at 687 eV (Fig. 7c) that PVDF is present on the surface of the LFP particle. The quantity of PVDF on the surface of the modified sample was 3% (w/w) (Fig. 7d). The binder also remains after prolonged sputtering, suggesting that PVDF found in the bulk is co-deposited with $LiFePO_4$, while a shift to lower binding energy is observed. After a sputtering time of 2 min, 1% (w/w) of PVDF was found in the bulk (Fig. 7d). Further sputtering, up to 16 min, resulted in similar amount of PVDF in the bulk of the sample.

While TOFSIMS is not directly a quantitative technique, its extremely low detection limit, ease of elemental identification, and imaging capability make it an obvious choice as an analytical tool for the surface analysis of multicomponent solid systems.

Species of Li, Fe (from $LiFePO_4$), C and CF_n (fragments from PVDF) have been detected in the positive-ion mass spectra obtained from the surface of the modified EPD-LFP electrode. The individual-ion and total-ion images (50 μm × 50 μm) were normalized in such a way that the lowest measured intensity corresponds to the darkest color and the highest intensity to the brightest one. With the goal of determining the lateral distribution of the active-material particles and binder, and other additives used to prepare the EPD-LFP composite cathode, the TOFSIMS tests were carried out both in the negative (Fig. 8a–c) and positive-ion modes. To obtain higher ionic yield and better resolution, we analyzed the negative-ion images of the electrode after very brief Cs^+ sputtering (cleaning of the surface). The ionic species found – FeO^-, PO_2^-, F^-, C^- and C^{2-} are representative of $LiFePO_4$, PVDF and carbon respectively. Ion images show that the cathode has a porous structure. Li, Fe and PO_2 species-rich regions may indicate the formation of aggregates of $LiFePO_4$ during the EPD process. PVDF fills the pores between single particles and aggregates of LFP, but also coats their surface. Filling of the pores is evidenced by the alternating appearance of FeO/PO_2 and F-species signals in the line scan across the sample surface (Fig. 8b). The distribution of BP carbon was found to be insufficiently uniform (Fig. 8a). Negative-ion images of the surface of the CuS-coated LFP cathode are shown in Fig. 8c. Surface mass spectra show strong S signal, while PO and PO_2 ions are not seen, indicating quite tight coverage of the $LiFePO_4$ surface by copper sulfide. This is in a good agreement with the SEM image (Fig. 3), in which copper sulfide completely covers the lithium iron phosphate-based composite electrode. On the other hand, in the positive-ions mode the intensity of the TOFSIMS signal arising from lithium was found to

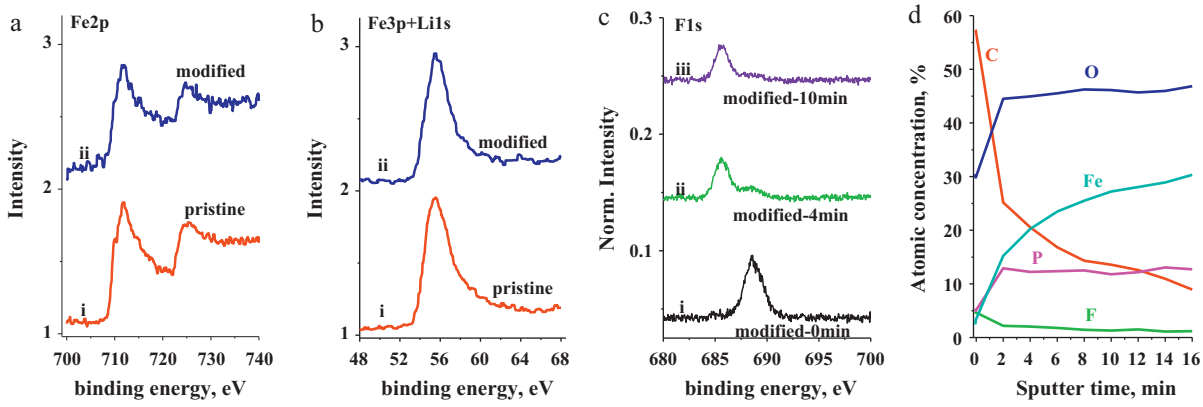

Fig. 7. XPS spectra of (a) Fe2p spectra for pristine and modified LFP samples; (b) Fe3p + Li1s spectra for pristine and modified LFP samples; (c) F1s spectra of modified LFP sample at various sputtering times and (d) depth profile of modified LFP sample.

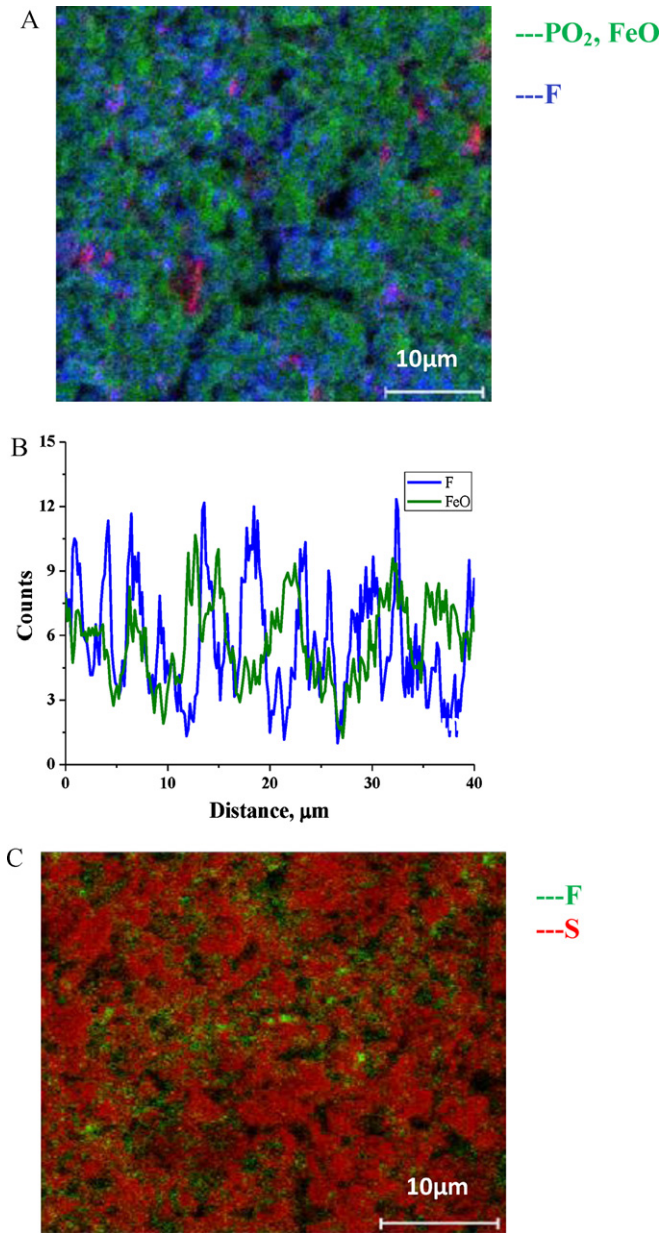

Fig. 8. TOFSIMS images of planar LFP cathodes; (a) negative surface ion-imaging of modified (PVDF and TTX-100), (b) line scan across sample surface of modified (PVDF and TTX-100), and (c) negative surface ion-imaging of modified (PVDF and TTX-100) cathode coated by thin-film CuS.

be much stronger than that of copper (not shown here). This points towards the formation of very thin top coating. Fluorine is present in the mass spectra and in the ion images at some points between the grains/aggregates of the active cathode material. Obviously, where the binder is present, CuS is not deposited.

We cannot state that this layer is stoichiometric or non-stoichiometric copper sulfide, or even a mixture of CuS and Cu_2S. However, in our case, this is not important, since both sulfides are characterized by high electron conductivity and can serve as a matrix for Li^+ insertion/deinsertion.

3.1. Electrochemical characterization

Table 1 displays the content of LFP EP-deposited samples' "a"–"f" bath composition. Samples a–c, e and f were electrophoretically deposited (EP) on a planar (2D) Ni substrate. Pristine, sample a,

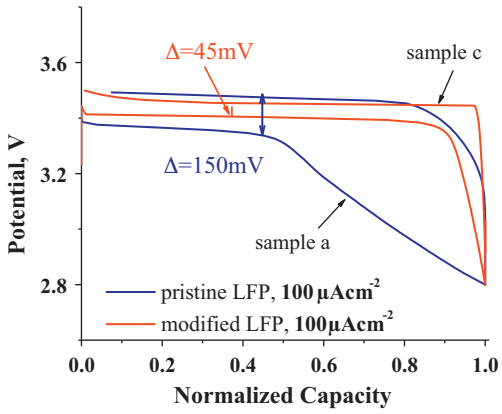

Fig. 9. Charge–discharge curves of 2D pristine (sample a) and 2D modified (sample c) LFP cells at current density of 0.1 mA cm^{-2}.

was EP-deposited from a colloidal suspension that included $LiFePO_4$ commercial powder. Sample b was modified with black-pearl carbon, while sample c was modified with black-pearl carbon, PVDF binder and TTX-100 surfactant. Samples d and g were EP-deposited on a gold-coated perforated-silicon substrate (3D) with an area-gain (AG) of 9 and content similar to that of sample c. Samples e and f were coated by copper sulfide on nickel and gold-coated silicon substrates, respectively.

Fig. 9 shows the comparative charge–discharge curves of EP-deposited planar pristine (a) and modified (c) samples at a current density of 0.1 mA cm^{-2}. As can be seen from this graph, the incorporation of additives to the LFP cathode lowered the polarization. The pristine cell exhibited 150 mV charge/discharge overpotential, a value more than three times that observed for the modified LFP cell. In addition, the discharge profile of the modified LFP cell follows a well-defined voltage plateau at 3.3 V throughout discharge, while a sloping character is observed for the pristine LFP cell. In agreement with the suggestion of Guyomard [33] we believe that the addition of the non-ionic surfactant Triton X-100 to the suspension used for the preparation of the EPD-LFP cathode favored a more homogeneous distribution of carbon black. This in turn, resulted in a better electronic wiring of the active material particles and lower internal resistance of the cells. The tenth discharge curves of samples a–c are shown in Fig. 10a. Sample modification with BP carbon (sample b) showed improved performance (~155 mAh g^{-1}) in comparison to non-modified sample a (~10 mAh g^{-1}). Modification of the LFP cathode with PVDF, BP carbon and TTX-100 (sample c) resulted in the best performance of the planar cell. The discharge specific capacity of 163 mAh g^{-1} is very close to the theoretical specific capacity of $LiFePO_4$ (170 mAh g^{-1}). The improved cycling performance can be attributed to the uniform crystalline phase of the $LiFePO_4$ EPD film (confirmed by XRD), good adhesion of the LFP particles to the gold-plated silicon substrate and improved electronic conductivity by carbon contacts. The voltage plateau remained flat through prolonged charge/discharge cycling of the cells with modified cathodes (Fig. 10a), samples b and c). It is worth mentioning that electrophoretic deposition can be utilized for the preparation of relatively thick LFP cathodes. For example, planar $LiFePO_4$/Li cells with modified LFP cathodes deposited at 100 V for 120 s showed a reversible capacity of about 1 mAh cm^{-2}.

The cycling performance of the various LFP samples was evaluated by cycling at the 0.1–0.5*C* rate or 0.05–0.2 mA cm^{-2} (battery footprint) at room temperature (Fig. 10b and c). Some irregularities are noticed for the discharge-capacity values of sample d at different cycle numbers (Fig. 10c). This phenomenon repeats itself randomly during prolonged cycling of the cell and is possibly due to electronic disconnections between the LFP particles. This can be

Table 1
Content list of the $LiFePO_4$ samples a → f.

Sample	$LiFePO_4$ (%w/w)	BP Carbon (%w/w)	PVDF (%w/w)	TTX-100 (%v/v)	Cell type
a	100	0	0	0	2D Li/LFP on Ni substrate
b	96	4	0	0	2D Li/LFP on Ni substrate
c	91	4	5	0.8	2D Li/LFP on Ni substrate
d	91	4	5	0.8	Semi-3D Li/LFP on Au-coated Si
e	91	4	5	0.8	2D Li/CuS-coated LFP on Ni substrate
f	91	4	5	0.8	Semi-3D Li/CuS-coated LFP on Au-coated Si

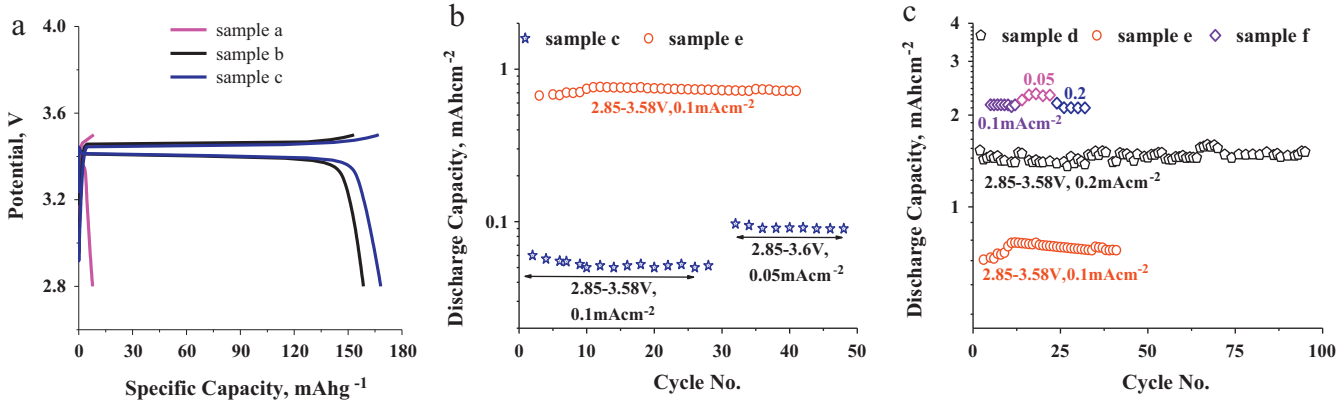

Fig. 10. (a) Voltage profiles of Li vs. LFP 2D cells (samples a → c) at 10th cycle, (b) Electrochemical cycling performance of samples c → e at various *C*-rates and voltage cutoffs and (c) electrochemical cycling performance of samples d → f at various *C*-rates and voltage cutoffs.

overcome by coating the LFP particles with a thin film of conducting material, in this case, CuS (Fig. 10b, sample e). Copper sulfide is known for its high electronic conductivity of 10^{-3}–0.1 S cm^{-1} [34]. The more uniform distribution of electrodeposited CuS between LFP particles than that of BP carbon additive, leads to lower polarization and, consequently, to higher reversible capacity at a given voltage cut-off of the battery. As can be seen from the graph of sample e (Fig. 10b), coating the cathode with CuS resulted in a more uniform particle distribution and capacity enhancement by a factor of 7 in comparison to modified sample c (not coated with CuS).

The cycling performance of the semi-3D modified LFP cell (Fig. 10c, sample d) was also evaluated. The modified semi-3D LFP cell (Fig. 10c, sample d) had about 1.5 mAh cm^{-2} (battery footprint) reversible capacity and the capacity values were stable for 100 cycles with a degradation rate of 0.01% capacity loss per cycle. Consecutively, the capacity of the planar cell with a modified cathode (Fig. 10b, sample c) comprising of similar composition to that of the modified semi-3D LFP cell (Fig. 10c, sample d), was about 0.1 mAh cm^{-2} at 0.5*C*. This agrees with the geometrical-area gain (AG = 9) of the perforated silicon substrate. The best cycling performance was that of the cell with a CuS-coated LFP cathode (Fig. 10c, sample f), which had a discharge capacity of 2.3 mAh cm^{-2} at 0.05 mA cm^{-2} or 0.02*C*. The electrode with the CuS topcoat had a higher capacity than the one without coating both at low and high charge/discharge rates.

Fig. 11 shows polarization curves of modified 2D (sample c) and modified semi-3D (sample d) cells with electrophoretically deposited LFP cathode. Both cathodes were deposited under similar conditions and both contained LFP, black-pearl carbon, PVDF binder (ratio 91:4:5% (w/w)) and TTX-100. The pulse duration was one second followed by a rest period of 20 s. As can be seen from the graph, the transition from 2D to 3D architecture is followed by an increase in maximum current-density capability from 30 to 75 mA cm^{-2}. The semi-3D cells on perforated-silicon substrate and CuS-coated modified LFP electrodes (Fig. 11, sample f) were able to provide more than 85 mA cm^{-2} current density and 204 mW cm^{-2}

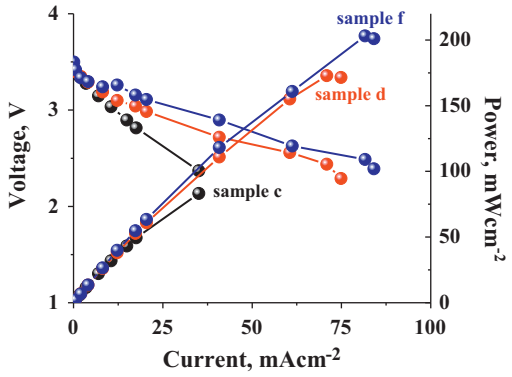

Fig. 11. Polarization curves of modified 2D (sample c) and modified semi-3D (samples d and f) Li/LFP cells.

peak power of battery footprint, a 24% increase over the semi-3D non-CuS-coated LFP cell (sample d) and a significant enhancement in comparison to the 2D LFP cell architecture.

The cell with a CuS–$LiFePO_4$ cathode outperforms the power capability of the cell containing a modified LFP cathode. Notwithstanding the fact that the typical voltage cutoff used for cycling Li/LFP-CuS cells is 2 V higher than that for the pristine Li/CuS cells [10], we suggest that in addition to its high electron conductivity, copper sulfide assists in the insertion/deinsertion of lithium ion in $LiFePO_4$ and provides better access of Li^+ to active material sites.

4. Conclusions

Three-dimensional cathode structure ensures overall electrode conductivity, facilitates lithium diffusion in and out of the $LiFePO_4$ particles and thus enables good cycling stability at the 1*C* rate and maximum pulse-power that exceeds that of planar $LiFePO_4$ electrodes at high electrode loading. Cathodes modified with PVDF and

black-pearl carbon outperform pristine cathodes. We have shown that a CuS top-coat on the LFP particles is crucial for obtaining better cathode performance. This is due to more uniform distribution around each active LFP particle and results in lower polarization. In terms of cathode performance, the cell with CuS-coated LFP cathode, outperforms the power capability of non-coated LFP cell. The high-power capability of the CuS-coated LFP cathode combined with its high reversible capacity, makes this cathode a promising candidate for high-power and high-energy MB applications.

References

[1] J.W. Lon, B. Dunn, D.R. Rolison, H.S. White, Chem. Rev. 104 (2004) 4463–4492.
[2] J.B. Bates, N.J. Dudney, B. Neudecker, A. Ueda, C.D. Evans, Solid-State Ionics 135 (2000) 33–45.
[3] R. Hart, H. White, B. Dunn, D.R. Rolison, Electrochem. Commun. 5 (2003) 120.
[4] M. Nathan, E. Peled, D. Haronian, Microelectrochemical cell, US, Patent No. 6,197,450.
[5] A. Averbuch, M. Nathan, I. Sedelnikova, J. Power Sources 196 (2011) 1521–1529.
[6] M. Nathan, D. Golodnitsky, V. Yufit, E. Strauss, T. Ripenbein, I. Shechtman, S. Menkin, E. Peled, J. Microelectromech. Syst. 14 (2005) 879.
[7] D. Golodnitsky, V. Yufit, M. Nathan, I. Shechtman, T. Ripenbein, E. Strauss, S. Menkin, E. Peled, J. Power Sources 153 (2006) 281.
[8] D. Golodnitsky, M. Nathan, V. Yufit, E. Strauss, T. Ripenbein, I. Shechtman, S. Menkin, L. Burstein, A. Gladkich, E. Peled, Solid-State Ionics 177 (2006) 2811.
[9] N.J. Dudney, Electrochem. Soc. Interface 17 (2008) 44–48.
[10] H. Mazor, D. Golodnitsky, L. Burstein, E. Peled, Electrochem. Solid-State Lett. 12 (2009) A232–A235.
[11] V. Yufit, K. Freedman, M. Nathan, L. Burstein, D. Golodnitsky, E. Peled, Electrochim. Acta 50 (2004) 417–420.
[12] A.K. Padhi, K.S. Nanjundaswamy, J.B. Goodenough, J. Electrochem. Soc. 144 (1997) 1188.
[13] M. Thackeray, Nat. Mater. 1 (2002) 81.
[14] A. Yamada, S.C. Chung, K. Hinokuma, J. Electrochem. Soc. 148 (2001) A224.
[15] L. Damen, J. Hassoun, M. Mastragostino, B. Scrosati, J. Power Sources 195 (2010) 6902–6904.
[16] D. Wang, H. Li, S. Shi, X. Huang, L. Chen, Electrochim. Acta 50 (2005) 2955–2958.
[17] C. Delacourt, P. Poizot, S. Levasseur, C. Masquelier, Electrochem. Solid-State Lett. 9 (2006) A352.
[18] F. Croce, A.D. Epifanio, J. Hassoun, A. Deptul, T. Olczac, B. Scrosati, Electrochem. Solid-State Lett. 5 (2002) A47.
[19] N. Hua, C. Wang, X. Kang, T. Wumair, Y. Han, J. Alloys Compd. 503 (2010) 204.
[20] J. Hu, J. Xie, X. Zhao, H. Yu, X. Zhuo, G. Cao, J. Tu, J. Mater. Sci. Technol. 25 (2009).
[21] P.P. Prosini, D. Zane, M. Pasquali, Electrochim. Acta 46 (2001) 3517.
[22] Y. Jin, C.P. Yang, X.H. Rui, T. Cheng, C.H. Chen, J. Power Sources 196 (2011) 5623–5630.
[23] G.X. Wang, L. Yang, Y. Chen, J.Z. Wang, S. Bewlay, H.K. Liu, Electrochim. Acta 50 (2005) 4649–4654.
[24] I. Boyano, J.A. Blazquez, I. de Meatza, M. Bengoechea, O. Miguel, H. Grande, Y. Huang, J.B. Goodenough, J. Power Sources 195 (2010) 5351–5359.
[25] E. Jing, H. Tong, L. Kong, C. Wang, Appl. Phys. A 80 (2005) 597–600.
[26] K. Kanamura, A. Goto, Y.H. Rho, T. Umegaki, J. Power Sources 97–98 (2001) 294–297.
[27] O.O. Van der Biest, L.J. Vandeperre, Annu. Rev. Mater. Sci. 29 (1999) 327–352.
[28] R. Dominko, M. Gaberscek, J. Drofenik, M. Bele, S. Pejovnik, J. Jamnik, J. Power Sources 119–121 (2003) 770–773.
[29] A. Kumar, R. Thomas, N.K. Karan, J.J. Saavedra-Arias, M.K. Singh, S. Majumder, M.S. Tomar, R.S. Katiyar, J. Nanotechnol. (2009), Article ID 176517.
[30] Y.H. Rho, L. Nazar, L. Perry, D. Ryan, J. Electrochem. Soc. 154 (2007) A283–A289.
[31] M. Herstedt, M. Stjerndahl, A. Nyten, T. Gustafsson, H. Rensmo, H. Siegbahn, N. Ravet, M. Armand, J.O. Thomas, K. Edstrom, Electrochem. Solid-State Lett. 6 (2003) A202–A206.
[32] C.D. Wagner, A.V. Naumkin, A. Kraut-Vass, J.W. Allison, C.J. Powelland, J.R. Rumble, NIST X-Ray Photoelectron Spectroscopy Database, http://srdata.nist.gov/xps/2003.
[33] W. Porchera, B. Lestriez, S. Jouanneaua, D. Guyomard, J. Power Sources 195 (2010).
[34] H. Grijalva, M. Inoue, S. Boggavarapu, P. Calvet, J. Mater. Chem. 6 (1996) 1157–1160.